Supporting Information

Day et al. 10.1073/pnas.0809645106

SI Text

Construct Design. IMAGE consortium clones used were: clone ID MGC2316 (cyclin D1) and clone ID MGC19704 (CDK4) (1) (Geneservice Ltd) were used for initial construct generation. See Fig. S1.

Coexpression of full-length, CDK4 (residues 1–303), with a C-terminal hexa-histidine tag, and cyclin D1 (residues 1–295) in insect cells yielded an enzymatically-active complex that had heterogeneous phosphorylation of both CDK4 and cyclin D1, and failed to crystallize. Introduction of T172A (CDK4) and T286A (cyclin D1) substitutions yielded a nonphosphorylated complex that also failed to crystallize. Subsequently cyclin D1 was C-terminally truncated (CycD1$_{1-271}$) to remove the Thr-286 phosphorylation site and flexible polyglutamate PEST region, and the hepta-glycine loop of CDK4 (residues 42–48) was replaced with Gly$_{42}$-Glu$_{43}'$-Glu$_{44}'$-Gly$_{48}$ (CDK4$_{EE}$), the sequence found in CDK6. See Fig. S1.

The CDK4$_{EE}$T172A/CycD1$_{1-271}$ complex yielded crystals diffracting to 2.8 Å and enabled a molecular replacement structure solution (see below). Novel crystallization conditions were also identified for CycD1$_{1-271}$ in complex with a phospho-mimetic construct CDK4$_{EE}$T172D and with a CDK4 construct containing phosphorylated T172 (CDK4$_{EE}$T172Ph). Data were collected to 2.3- and 2.9-Å resolution, respectively, for each of these complexes. The phosphorylation state of crystallized CDK4$_{EE}$Ph/CycD1$_{1-271}$ was confirmed by LC/MS analysis of dissolved complex crystals. All 3 of the complexes yielded equivalent structures. In all of these structures the N-terminal region of cyclin D1 was disordered. Thus a further truncation was designed (CycD1$_{15-271}$) that, in combination with CDK4$_{EE}$T172A, produced a complex that crystallized readily, even in the absence of precipitant, yielding a 2.5-Å resolution structure.

Protein Purification. CDK4$_{EE}$(1–303/His$_6$)/CycD1$_{1-271}$ was expressed in SF21 insect cells and harvested 72 h after infection. After sonication and clarification, the complex was purified by using Ni-NTA agarose batch binding, HitrapQ FF ion exchange chromatography, and gel filtration on a Sephacryl S200HR(26/60) column. The purified complex was typically concentrated to 10–12 mg/mL in 20 mM Tris·HCl (pH 8), 10% glycerol, 150 mM NaCl, 5 mM DTT for crystallization. All work was carried out at 4 °C.

Crystallization. *CDK4$_{EE}$T172A/CycD1$_{1-271}$.* Protein was concentrated to 12 mg/mL and mixed 1:1 with reservoir solution composed of 0.1 M Tris·HCl (pH 7.0), 10% (wt/vol) PEG4000, 0.2 M ammonium sulfate, and 1 mM AMP-PNP in sitting drops and incubated at 20 °C. Small plates appeared in 1–3 days. Crystals were cryoprotected in 0.1 M Tris·HCl (pH 7.0), 10% (wt/vol) PEG4000, 0.2 M ammonium sulfate, and 20% (vol/vol) glycerol before freezing in liquid nitrogen and collecting data.

CDK4$_{EE}$T172D/CycD1$_{1-271}$. Protein was concentrated to 10 mg/mL and mixed 1:1 with reservoir solution composed of 0.1 M Hepes (pH 7.5) and 0.5–0.8 M trisodium citrate in hanging drops and incubated at 20 °C. Large plates appeared in 1–3 days. Crystals were cryoprotected in 0.1 M Hepes (pH 7.5), 0.75 M trisodium citrate, and 20% (vol/vol) glycerol before freezing in liquid nitrogen and collecting data.

CDK4$_{EE}$T172Ph/CycD1$_{1-271}$. Protein was concentrated to 10 mg/mL and mixed 1:1 with reservoir solution composed of 1.0–1.5 M sodium potassium phosphate (pH 7.0–8.0) in hanging drops and incubated at 20 °C. Large plates appeared in 1–3 days. Crystals were cryoprotected in 1.2 M sodium potassium phosphate (pH 7.0–8.0) and 20–25% (vol/vol) glycerol before freezing in liquid nitrogen and collecting data.

CDK4$_{EE}$T172A/CycD1$_{15-271}$. Protein was concentrated to 3.3 mg/mL and mixed 1:1 with reservoir solution composed of 0.1 M Mes (pH 6.0) and 0–10% (vol/vol) 2-methyl-2,4-pentanediol in sitting drops and incubated at 20 °C. Showers of small plates appeared in 1–3 days. Crystals were cryoprotected in 0.1 M Mes (pH 6.0) and 25% (vol/vol) 2-methyl-2,4-pentanediol before freezing in liquid nitrogen and collecting data.

Structure Solution. All X-ray data were collected on beamlines ID23 and ID29 at the European Synchrotron Radiation Facility. The 2.85-Å dataset collected from crystals of construct CDK4$_{EE}$T172A/CycD1$_{1-271}$ were initially indexed as ($a = 57.15$, $b = 64.84$, $c = 188.97$ Å) P22$_1$2$_1$. PHASER (2) generated consistent rotation function (RF) solutions by using a variety of cyclin alignments, models, and ensembles. A weak RF solution was found for CDK4 by using the C-terminal domain of CDK6 (extracted from PDB ID code 1BLX, 1.9Å) as a search model, but no translation function (TF) solutions were found for all of the CDK and cyclin models tested. Data twinning tests proved negative and so TF solutions were sought in all 7 other orthorhombic space groups. P2$_1$2$_1$2$_1$ yielded excellent TF solutions for cyclin D1 and weak TF solutions for the CDK C-terminal domain model. Extensive attempts to find solutions for the CDK4 N-terminal domain failed. The spacegroup ambiguity was identified as being attributable to anisotropic mosaicity that had lead to an overlap of closely separated (h,0,−l), (h,0,0) and (h,0,l) spots. The CDK4/CycD1 crystals are plate-like and it is likely that the long c-axis is perpendicular to the plate and that the anisotropic mosaicity is caused by warping of the plate. The P2$_1$2$_1$2$_1$ molecular replacement solutions revealed new helical density proximal to the cyclin, which was thought to correspond to the kinase α1-helix. The validity of this solution was, however, questioned as it implied a radically different relative disposition of the CDK and cyclin subunits, as compared with other CDK/cyclin complexes. An independent molecular replacement solution was sought and found, but simply confirmed the previously identified solution. Again the N-terminal domain of the kinase could not be identified.

Because conventional molecular replacement had failed to locate the CDK4 N-terminal domain, an attempt was made to identify its location by using real space search methods. An ESSENS (3) search using polyAla search models constructed from the CDK6 N-terminal domain from PDB ID code 1BLX and CDK6 α1-helix from PDB ID code 1BLX yielded a plausible solution. Rigid body refinement of the hybrid model comprising the cyclin D1 N- and C-terminal domains, CDK4 N-terminal domain β-sheet polyAla model, CDK4 C-terminal domain (CDK6 molecular replacement solution), and polyAla α1-helix model gave $R = 0.544$.

At this time MIR data became available, although both the "new" native and derivative data sets were nonisomorphous with the original native. Model phased heavy-atom difference Fourier and MLPHARE (4) gave a 4-site solution for a PCMBS 3.7-Å derivative, although it had inadequate phasing power and resolution to enable an independent SIR(AS) map. Phase combination with the molecular replacement model phases gave a map of sufficient quality to enable initial model building. Subse-

quently, the original, higher-resolution, native dataset was used for iterative model rebuilding and refinement.

It proved possible to position the majority of main- and side-chain atoms in cyclin D1, but side-chain density was generally poor within CDK4. The difference in the quality of the electron density for the CDK4 and cyclin D1 subunits correlated with significantly elevated B factors in CDK4, with the exception of the α1-helix. Simulated annealing did not improve map quality. Initially the structure was manually rebuilt and refined by using Refmac (5), but Buster and autoBuster were used as refinement packages in the later stages of the refinement (6). Data collection and refinement statistics for the four structures determined are listed in Table S4.

Measurement of CDK Enzyme Activity. CDK enzyme activity was measured by using an ELISA format. Briefly, plates were coated with GST-pRb[769–921] (purified as described in ref. 7), washed with TBST [100 mM Tris (pH 7.5), 150 mM NaCl, 0.5% Tween-20], and blocked with Superblock (Perbio Science). Assay buffer [final concentrations: 15 mM $MgCl_2$, 50 mM Hepes (pH 7.4), 1 mM DTT, 1 mM EGTA (pH 8.0), 0.02% Triton X-100, and 2.5% DMSO] and enzyme [CDK4/CycD1 or CDK2(T160Ph)/CycA] were added to each well and the reaction was initiated with the addition of ATP. At various time points reactions were stopped by the addition of 0.5 M EDTA, pH 8.0. Plates were then washed with TBST and incubated for 1 h with the primary antibody (CDK4: anti-p-Rb Serine 780, New England Biolab; Cdk2: p-Rb Threonine 821, Biosource) diluted in Superblock. Excess antibody was washed off and plates were then incubated with secondary antibody (alkaline phosphatase-linked anti-rabbit; New England Biolab) for another hour. After removal of excess secondary antibody, plates were developed by using the Attophos system (Promega) and the fluorescence was read on a Spectramax Gemini plate reader (Molecular Devices) at excitation 450 nm and emission 580 nm.

The relative activities of the constructs were determined by measuring the initial rates of reaction for each construct in the presence of 2 mM ATP. Rates were then normalized relative to the wild-type construct.

rmsd Calculations for Kinase and Cyclin Overlays. PDB files were superposed by using Cα atoms in KFIT (software from I.J.T.). Atom pairs separated by $\leq$2 Å were included in calculations. The superposed cyclins are shown in Fig. S3. rmsd values for the cyclin and kinase superpositions are tabulated in Table S1 and Table S2 respectively.

Buried Surface Area Calculation and Contact Surfaces. Buried surface areas (Table S3) were calculated by using MAXBSA (software from I.J.T.). Contact surfaces were generated by using AREAIMOL (4) with a 1.4-Å probe radius and are shown in Fig. S5.

LC/MS of Dissolved CDK4$_{EE}$T172Ph/CycD1$_{1–271}$ Crystals. Three crystals were diluted from 1.5 M phosphate to water in 3 steps to a final volume of 15 μL. All crystalline material had dissolved after 1 h at 4 °C at which point the sample was diluted to 75 μL in 2% formic acid and analyzed by LC/MS.

LC Method. The method involves a 25-μl injection, 23-min run with a 13-min linear gradient from 0% B to 100% B. Solvents were: A - 0.2% formic acid, B - 60% isopropanol/0.2% formic

acid. LC column was a Phenomenex Luna C8 150 $\times$ 3 mm. Flow rate was 0.2 mL/min, column compartment temperature was 60 °C, and UV detection was at 220 nm. Eluate was fed directly in to the source of a Bruker Daltonics MicroTOF MS. Each injection was internally calibrated with Agilent Tunemix from $m/z = 322$ to 2,721.

Two adjoining peaks were observed at retention time = 15–16 min in both the UV and the total ion chromatogram traces. The first peak contained a major species mass 34,516.6 Da, corresponding to acetylated, monophosphorylated CDK4 $_{EE}$T172Ph with $\approx$14% of a second species, mass 34,435.9 Da, corresponding to nonphosphorylated CDK4 $_{EE}$T172. The second peak contained approximately equal amounts of 2 species mass 30,995.0 and 31,075.0 Da, corresponding to nonphosphorylated and monophosphorylated CyclinD1$_{15–271}$.

Sequences of CDK4 and Cyclin D1. For amino acid sequences of wild-type CDK4 and CyclinD1 (upper sequence) see Fig. S1. For reference the sequences for the mutated and truncated CDK4 and cyclin D1 constructs are listed below the wild-type sequences.

Discussion of Role of Cyclin N Terminus. We present structures for a CDK/cyclin D1 complex containing full-length cyclin D1 and also cyclin D1 that has a 15-aa N-terminal deletion. Both heterodimeric complexes are structurally equivalent, suggesting that the cyclin D1 N terminus alone cannot trigger a reconfiguration of the CDK4/cylcin D1 complex.

The CDK4/cyclin D1 complex containing truncated D1 cyclin has substantially reduced catalytic activity compared with the wild-type complex (Table 1). The reasons for this are not known. The N terminus of the cyclin contains a LxCxE Rb substrate binding motif. Deletion of this motif may alter the substrate specificity and/or activity of the CDK/cyclin complex (19–21). Activity was determined by using an ELISA format with antibodies against phospho-Ser-780 of a truncated Rb construct (GST-Rb 769–921). The kinase could potentially still have catalytic activity versus Rb, but with reduced phosphorylation of the site being probed (19–21). It could also be argued that the use of truncated Rb substrate may subtly modulate the selectivity/activity profile of the CDK/cyclin complex. Kinase activity may be genuinely reduced if the cyclin D1 N-terminal deletion has an impact on recruitment, binding, and orientation of the truncated Rb substrate (19–21). Mutational studies with the K-cyclin from herpesvirus (related to the D-type cyclins) have shown that the cyclin N terminus can modulate kinase substrate specificity (22). It should, however, be noted that the cyclin D1 LxCxE motif is not conserved in the viral cyclins.

The CDK4/cyclin D1 complexes presented have a similar overall conformation to the CDK9/cyclin T1 complex (18). The first 9 N-terminal amino acids of cyclin T1 are disordered and solvent exposed. Structures of CDK6 in complex with the vCyclin from herpesvirus saimiri, again related to the D-type cyclins, reveal the CDK6/vCyc complex to be in a fully active conformation (8). A similar active conformation is also observed in the structure of CDK2 complexed with a viral M-cyclin (16). In both structures the N terminus of the viral cyclin contacts and stabilizes the T-loop of the kinase. It is is, however, difficult to draw direct comparisons between the role of the cyclin D1 N terminus in our structures and the role of the V/M-cyclin N-termini because of the complexes adopting fundamentally different conformations and the lack of sequence conservation at the cyclin N-termini.

1. Lennon GG, et al. (1996) The I.M.A.G.E. Consortium: An integrated molecular analysis of genomes and their expression. *Genomics* 33:151–152.
2. McCoy AJ, Grosse-Kunstleve RW, Storoni LC, Read RJ (2005) Likelihood-enhanced fast translation functions. *Acta Crystallogr D* 61:458–464.
3. Kleywegt GJ, Jones TA (1997) Template convolution to enhance or detect structural features in macromolecular electron-density maps. *Acta Crystallogr D* 53:179–185.
4. Collaborative Computational Project No. 4 (1994) The CCP4 suite: Programs for protein crystallography. *Acta Crystallogr D* 50:760–763.

5. Murshudov GN, Vagin AA, Dodson EJ (1997) Refinement of macromolecular structures by the maximum-likelihood method. *Acta Crystallogr D* 53:240–255.
6. Blanc E, et al. (2004) Refinement of severely incomplete structures with maximum likelihood in BUSTER-TNT. *Acta Crystallogr D* 60:2210–2221.
7. Wu JJ, et al. (2000) Measurement of cdk4 kinase activity using an affinity peptide-tagging technology. *Comb Chem High Throughput Screen* 3:27–36.
8. Schulze-Gahmen U, Kim S-H (2002) Structural basis for CDK6 activation by a virus encoded cyclin. *Nat Struct Biol* 9:177–181.
9. Brown NR, et al. (1999) The structural basis for specificity of substrate and recruitment peptides for cyclin-dependent kinases. *Nat Cell Biol* 1:438–443.
10. Russo AA, Jeffrey PD, Pavletich NP (1996) Structural basis of cyclin-dependent kinase activation by phosphorylation. *Nat Struct Biol* 3:696–700.
11. Jeffery PD, Tong L, Pavletich NP (2000) Structural basis of inhibition of cdk-cyclin complexes by INK4 inhibitors. *Genes Dev* 14:3115–3125.
12. Brotherton DH, et al. (1998) Crystal structure of the complex of the cyclin D-dependent kinase Cdk6 bound to the cell-cycle inhibitor p19[INK4d]. *Nature* 395:244–250.
13. Russo AA, et al. (1998), Structural basis for inhibition of the cyclin-dependent kinase Cdk6 by the tumor suppressor p16INK4a. *Nature* 395:237–243.
14. Lolli G, et al. (2004) The crystal structure of human CDK7 and its protein recognition properties. *Structure (London)* 12:2067–2079.
15. De Bondt HL, et al. (1993) Crystal structure of cyclin-dependent kinase 2. *Nature* 363:595–602.
16. Card GL, et al. (2002) Crystal structure of a γ-herpesviruscyclin–cdk complex. *EMBO J* 19:2877–2888.
17. Honda R, et al. (2005) The structure of cyclinE1/Cdk2: Implications for cdk2 activation and cdk2-independent roles. *EMBO J* 24:452–463.
18. Baumli S, et al. (2008) The structure of P-TEFb (CDK9/cyclinT1), its complex with flavopiridol and regulation by phosphorylation. *EMBO* 27:1907–1918.
19. Grafstrom RH, et al. (1999) Defining the substrate specificity of cdk4 kinase-cyclin D1 complex. *Carcinogenesis* 20:193–198.
20. Wallace M, Ball K. (2004) Docking-dependent regulation of the Rb tumor suppressor protein by Cdk4. *Mol Cell Biol* 24:5606–5619.
21. Pan W, et al. (1998) Defining the minimal portion of the retinoblastoma protein that serves as an efficient substrate for cdk4 kinase/cyclin D1 complex. *Carcinogenesis* 19:765–769.
22. Kaldis P (2005) The N-terminal peptide of the Kaposi's sarcoma-associated herpesvirus (KSHV)-cyclin determines substrate specificity. *J Biol Chem* 280:11165–11174.
23. Li M, et al. (1997) Kaposi's sarcoma-associated herpesvirus encodes a functional cyclin. *J Virol* 71:1984–1991.

CDK4

1
```
MATSRYEPVAEIGVGAYGTVYKARDPHSGHFVALKSVRVPNGGGGGGGGLPISTVREVALL
MATSRYEPVAEIGVGAYGTVYKARDPHSGHFVALKSVRVPNGE---EGLPISTVREVALL
```

61
```
RRLEAFEHPNVVRLMDVCATSRTDREIKVTLVFEHVDQDLRTYLDKAPPPGLPAETIKDL
RRLEAFEHPNVVRLMDVCATSRTDREIKVTLVFEHVDQDLRTYLDKAPPPGLPAETIKDL
```

122
```
MRQFLRGLDFLHANCIVHRDLKPENILVTSGGTVKLADFGLARIYSYQMALTPVVVTLWY
MRQFLRGLDFLHANCIVHRDLKPENILVTSGGTVKLADFGLARIYSYQMAL*PVVVTLWY
```

183
```
RAPEVLLQSTYATPVDMWSVGCIFAEMFRRKPLFCGNSEADQLGKIFDLIGLPPEDDWPR
RAPEVLLQSTYATPVDMWSVGCIFAEMFRRKPLFCGNSEADQLGKIFDLIGLPPEDDWPR
```

244
```
DVSLPRGAFPPRGPRPVQSVVPEMEESGAQLLLEMLTFNPHKRISAFRALQHSYLHKDEG
DVSLPRGAFPPRGPRPVQSVVPEMEESGAQLLLEMLTFNPHKRISAFRALQHSYLHKDEG
```

305
```
NPE------
NPEHHHHHH
```

Cyclin D1

1
```
MEHQLLCCEVETIRRAYPDANLLNDRVLRAMLKAEETCAPSVSYFKCVQKEVLPSMRKIV
MEHQLLCCEVETIRRAYPDANLLNDRVLRAMLKAEETCAPSVSYFKCVQKEVLPSMRKIV
M-------------AYPDANLLNDRVLRAMLKAEETCAPSVSYFKCVQKEVLPSMRKIV
```

61
```
ATWMLEVCEEQKCEEEVFPLAMNYLDRFLSLEPVKKSRLQLLGATCMFVASKMKETIPLT
ATWMLEVCEEQKCEEEVFPLAMNYLDRFLSLEPVKKSRLQLLGATCMFVASKMKETIPLT
ATWMLEVCEEQKCEEEVFPLAMNYLDRFLSLEPVKKSRLQLLGATCMFVASKMKETIPLT
```

122
```
AEKLCIYTDNSIRPEELLQMELLLVNKLKWNLAAMTPHDFIEHFLSKMPEAEEENKQIIRK
AEKLCIYTDNSIRPEELLQMELLLVNKLKWNLAAMTPHDFIEHFLSKMPEAEEENKQIIRK
AEKLCIYTDNSIRPEELLQMELLLVNKLKWNLAAMTPHDFIEHFLSKMPEAEEENKQIIRK
```

183
```
HAQTFVALCATDVKFISNPPSMVAAGSVVAAVQGLNLRSPNNFLSYYRLTRFLSRVIKCD
HAQTFVALCATDVKFISNPPSMVAAGSVVAAVQGLNLRSPNNFLSYYRLTRFLSRVIKCD
HAQTFVALCATDVKFISNPPSMVAAGSVVAAVQGLNLRSPNNFLSYYRLTRFLSRVIKCD
```

244
```
PDCLRACQEQIEALLESSLRQAQQNMDPKAAEEEEEEEEEEVDLACTPTDVRDVDI
PDCLRACQEQIEALLESSLRQAQQNMDPKAA-------------------------
PDCLRACQEQIEALLESSLRQAQQNMDPKAA-------------------------
```

Fig. S1. CDK4 and cyclin D1 sequence alignments. Mutations are underlined, and truncations/extensions are represented by dashes. * = A, D, or phosphoT

Fig. S2. Lambda-phosphatase treatment. CDK4/cyclin D1 (10 μM) was incubated with 100 units of lambda phosphatase at 30 °C for 1 h in the presence or absence of 10 mM sodium orthovanadate in the manufacturer's buffer. Reactions were stopped by the addition of 10 mM sodium orthovanadate. Remaining activity was assessed by monitoring phosphorylation of GST-Rb808-836 at position 821 by Western blot analysis. Assay conditions were CDK4/cyclinD1 (50 nM), GST-Rb808−836 (50 μM), ATP (2.5 mM), MgCl$_2$ (10 mM) in assay buffer [20 mM Tris·HCl (pH 8), 150 mM NaCl, 10% glycerol, 5 mM DTT incubated at 25 °C for 1 h].
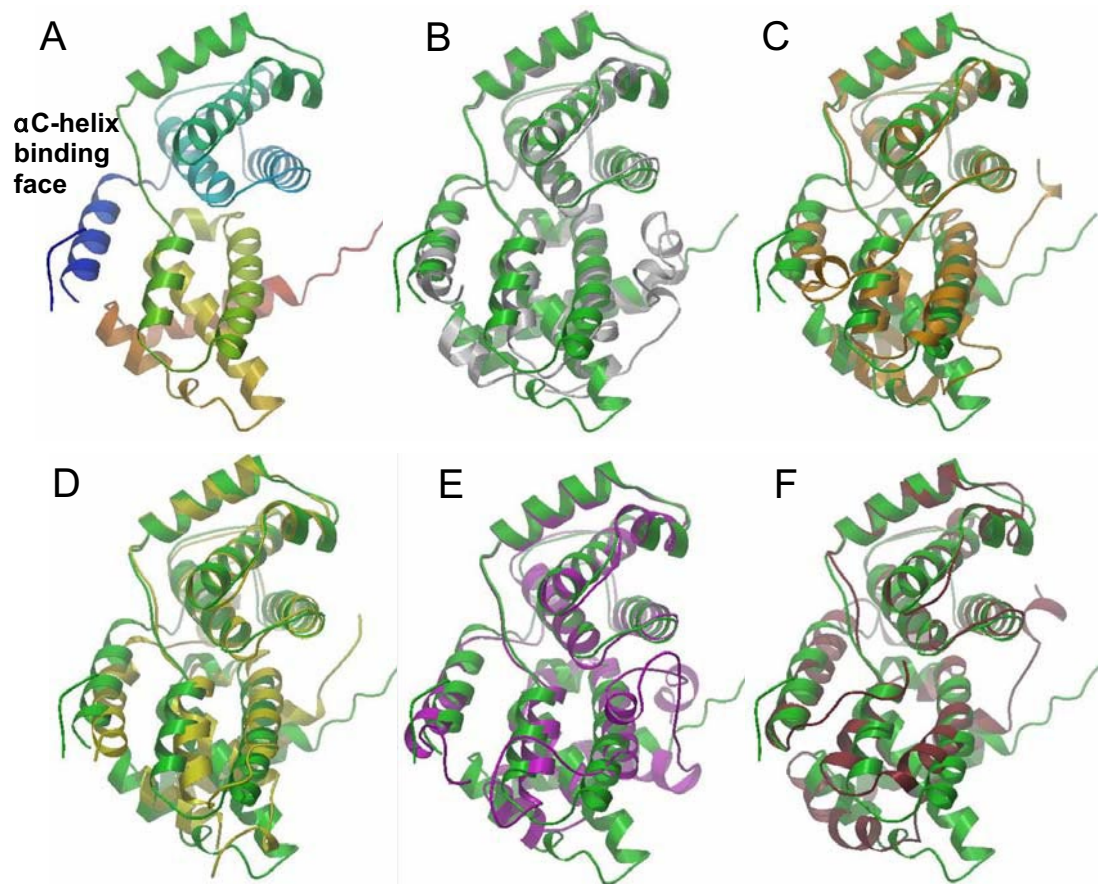
Fig. S3. Superposition of cyclins. (*A*) Cyclin D1 is colored by ''rainbow'' from N terminus (blue) to C terminus (red). The α1-helix recognition site is indicated. (*B–F*) Cyclin D1 (green) superposed with cyclin A3 (white), vCyclin (orange), cyclin K (yellow), cyclin E (purple), cyclin M (brown). Cyclin D1 is identically orientated in all 6 panels.
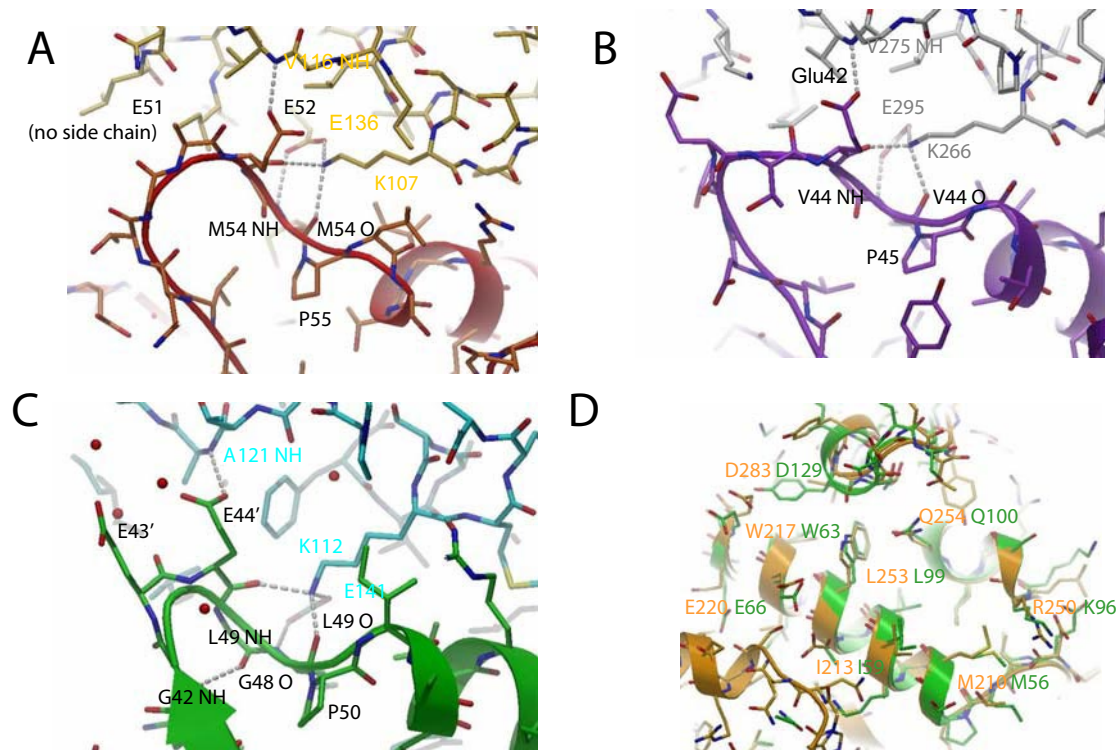
Fig. S4. CDK loop architecture preceding the α1-helice and inter-comparison of cyclin peptide recruitment sites. (*A*) Architecture of the loop preceding the α1-helix in the CDK6 (red)/vCyclin (orange) complex (PDB ID code1JOW). The apex of the loop is stabilized by hydrogen bonds from the loop main chain to a lysine and glutamate on the vCyclin. The side chain of the second glutamate within the loop GEEG motif provides additional stabilizing hydrogen-bonding interactions. (*B*) Architecture of the loop preceding the α1-helix in the CDK2 (purple)/cyclin A (gray) structure (PDB ID code 1QMZ). The apex of the loop is again stabilized by hydrogen bonds from the loop main chain to a highly conserved lysine and glutamate on the cyclin. A glutamate within the loop again provides additional stabilizing hydrogen-bonding interactions. (*C*) Architecture of the engineered loop preceding the α1-helix in the CDK4 (green)/cyclin D1 (cyan) structure. Akin to CDK2 and CDK6 the apex of the loop is stabilized by hydrogen bonds from the loop main chain to a highly conserved lysine and glutamate on the cyclin. The second glutamate from the GEEG insertion mimics the interactions formed by the glutamate in the CDK6 structure. The loop is further stabilized by intramolecular H-bonds, which are not observed in either the CDK2 or CDK6 structures. (*D*) Overlay of cyclin A (orange) (from PDB ID code 1QMZ; rmsd 0.84 Å) with cyclin D1 (green) in the vicinity of the cyclin A peptide recruitment site. Residues from cyclin A that are known to be important for peptide binding and the equivalent residues in cyclin D1 are labeled in orange and green, respectively.
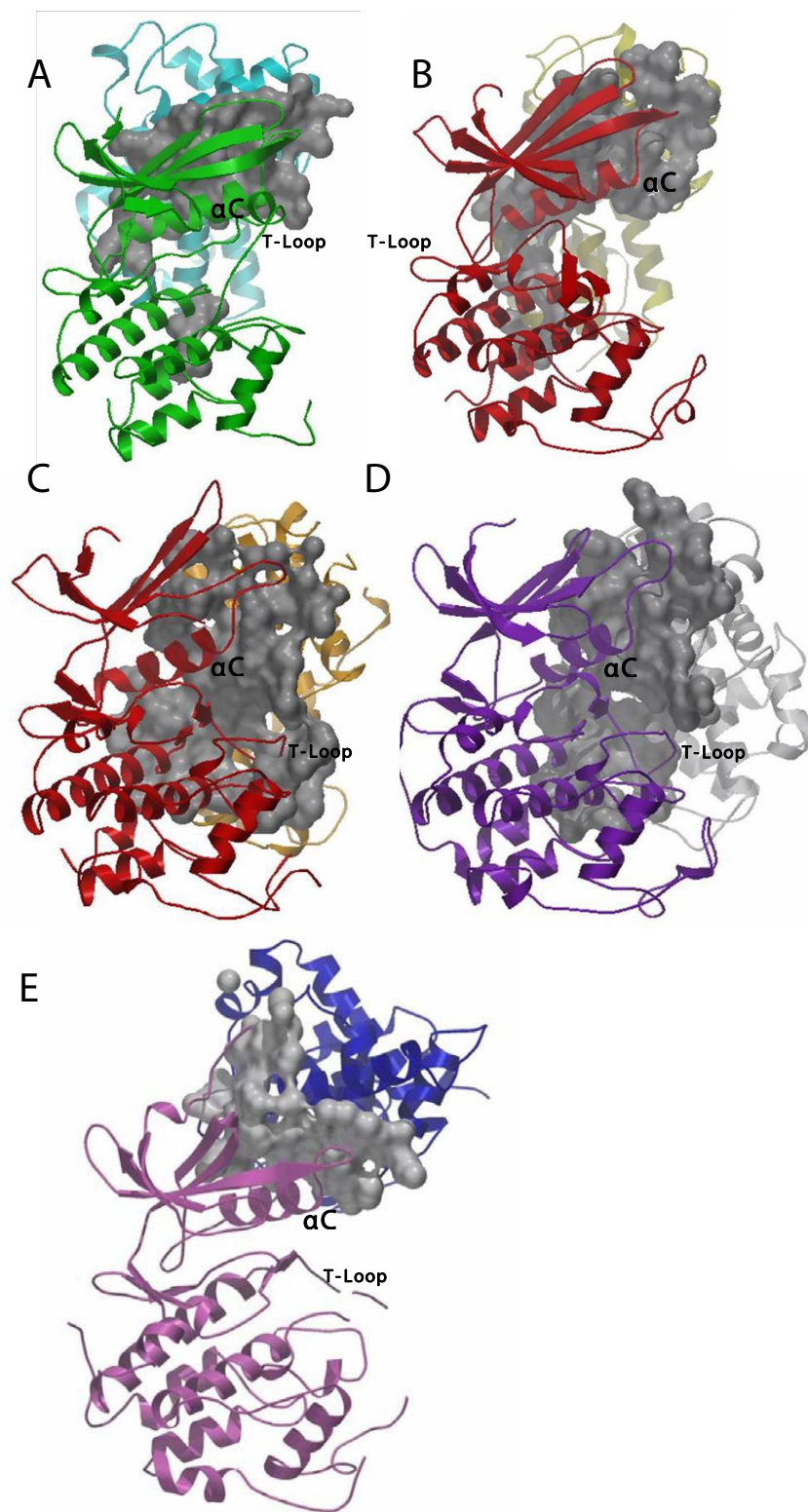
Fig. S5. Contact surfaces (gray) [calculated by using AREAIMOL (4)] for various CDK/cyclin complexes. (*A*) CDK4/cyclin D1 (green/cyan). (*B*) CDK6/KCyc (INK4c omitted for clarity) (PDB ID code 1G3N) (red/yellow/omitted). (*C*) CDK6/vCyc (PDB ID code 1JOW) (red/orange). (*D*) CDK2/CycA (PDB ID code 1QMZ) (purple/gray). (*E*) CDK9/CycT1 (PDB ID code 3BLH) (pink/blue) In the active complexes (*C* and *D*) it can be seen that the cyclins form extensive contacts with both the N- and C-terminal lobes of the kinases and the kinase activation loops. The CDK4/cyclin D1 interface is most reminiscent of the CDK/cyclin interfaces in the CDK6/Kcyc/INK4c and CDK9/cyclin T1 structures. In both of these systems the cyclin predominantly contacts the N-terminal lobe of the kinase and the contact area of the interface is reduced compared with other CDK/cyclin complexes.
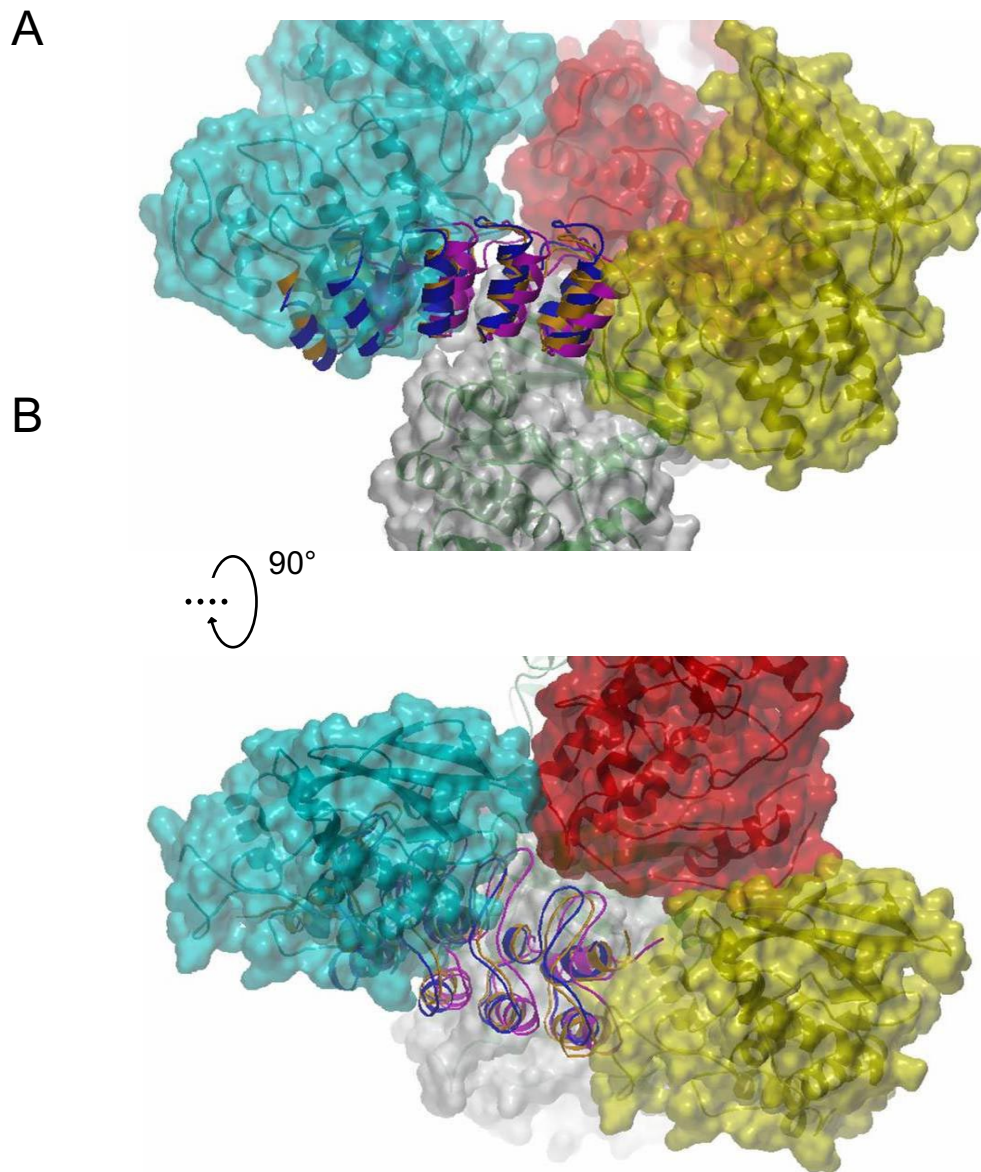
Fig. S6. CDK4/cyclin D1 structure crystal packing. (*A*) The CDK4 reference molecule (CycD1 not shown for clarity) is depicted as a green ribbon trace with a semitransparent gray surface. Symmetry-related molecules contacting the N-terminal domain of the reference CDK4 molecule are drawn as yellow, cyan, and red ribbon traces and semitransparent surfaces. Also shown are ribbon traces of p18INK4c (blue; PDB ID code 1G3N), p19INK4d (orange; PDB ID code 1BLX), and p16INK4a (pink; PDB ID code 1BI7) orientated by superposition of the CDK6 from each of these structures onto the CDK4 reference molecule. The superposition reveals that a significant portion of each of the INK molecules lies within the interstitial spaces of the CDK4/cyclin D1 crystal, which suggests that if CDK4 binds INK proteins in a manner comparable to CDK6 any putative CDK4/INK contact surface is not being mimicked by lattice contacts within the CDK4/cyclin D1 crystal. (*B*) As in *A* but rotated by 90° about the axis shown.

Table S1. Cyclin alignments with cyclinD1

Cyclin aligned	PDB ID code	Ref.	rmsd, Å (from KFIT)	No. of Cα atom pairs
CDK6/KCyc/INK4c	1G3N	11	0.901	157
CDK6/vCyc	1JOW	8	0.976	160
CDK2/MCyc	1F5Q	16	0.963	154
CDK2/CycE	1W98	10	1.000	158
CDK2/CycA	1JST	17	0.871	187
CDK2/CycA	1QMZ	9	0.840	188

Table S2. Kinase alignments with CDK4

Kinase aligned	PDB ID code	Ref.	rmsd, Å (from KFIT)	No. of Cα atom pairs
CDK6/vCyc	1JOW	8	1.114	183
CDK2/CycA	1QMZ	9	1.017	167
CDK2/CycA	1JST	10	0.858	146
CDK6/KCyc/p18INK4c	1G3N	11	0.888	189
CDK6/INK4d	1BLX	12	0.831	193
CDK6/p16INK4a	1BI7	13	0.797	166
CDK6/p19INK4d	1BI8	13	0.809	167
CDK7	1UA2	14	1.053	176
CDK2	1HCL	15	0.899	202
CDK9	1BLH	18	1.387	182

Table S3. Buried surface areas at the CDK/cyclin interface

Complex	PDB ID code	Ref.	Buried surface area, Å²) (from MAXBSA)
CDK4/CycD1			2,334
CDK6/KCyc/INK4c	1G3N	4	2,377
CDK6/vCyc	1JOW	1	3,974
CDK2/CycA	1QMZ	2	3,268
CDK2/CycA	1JST	3	3,266
CDK9/CycT1	1BLH	18	1,931

See references in Tables S1 and S2 for kinase and cyclin overlays section.

Table S4. Data collection and refinement statistics

Data Collection				
Crystal	$CDK4_{EE}T172D$ $CycD1_{1-271}$	$CDK4_{EE}T172A$ $CycD1_{1-271}$	$CDK4_{EE}T172Ph$ $CycD1_{1-271}$	$CDK4_{EE}T172A$ $CycD1_{15-271}$
Space group	$P2_12_12_1$	$P2_12_12_1$	$P2_12_12_1$	$P2_12_12_1$
Cell Dimensions a (Å)	55.9	57.0	58.0	57.198
b (Å)	64.7	64.7	64.3	65.011
c (Å)	168.7	188.7	187.6	188.699
Resolution (Å)	84.2–2.3	94.5–2.8	60.9–2.85	94.5–2.45
	(2.42–2.3)	(2.8–2.91)	(3.0–2.85)	(2.58–2.45)
Wavelength (Å)	0.931	0.940	0.931	0.931
Unique reflections	27793	17640	16778	26174
Redundancy	4.7	4.5		3.5
Completeness (%)	99.5(100)	98.6(94.8)	98.6(99.3)	98.4(99.4)
Mean $I/\sigma(I)$	5.2(1.5)	6.0(1.5)	5.7(1.9)	6.6(1.6)
R_{merge} (%)*	9.1(50.1)	8.8(53.5)	8.4(40.6)	7.5(41.6)
Refinement				
$R_{working}$[†]	20.4(21.2)	21.7(22.2)	22.8(20.4)	22.5(24.5)
R_{free}	26.1(25.0)	23.1(23.1)	30.4(25.4)	27.2(30.7)
No. atoms (protein)	4,095	4,369	3,966	4,240
No. atoms (water)	198	110	60	223
rmsd bonds (Å)	0.004	0.005	0.02	0.004
rmsd angles (°)	0.76	0.9	1.2	0.8
Average B factor (Å^2)				
Main chain	61.9	83.8	81.6	59.6
Side chain	69.9	92.2	84.1	68.7
Solvent	59.2	61.6	74.6	54.5

*$R_{merge} = \Sigma|I_I - (I)|/\Sigma I_i$, where I_i is the observed intensity and I is the mean intensity.
[†]$R_{working} = \Sigma\{|F_o| - |F_c|\}/\Sigma|F_o|$, where F_o is the observed structure factor amplitudes and F_c is the calculated structure factors.